LIMNOLOGY and OCEANOGRAPHY

ASLO

*Limnol. Oceanogr.* 9999, 2020, 1–17

doi: 10.1002/lno.11463

# Phosphonate cycling supports methane and ethylene supersaturation in the phosphate-depleted western North Atlantic Ocean

**Oscar A. Sosa**,[1,3*] **Timothy J. Burrell**,[1] **Samuel T. Wilson**,[1] **Rhea K. Foreman**,[1] **David M. Karl**,[1] **Daniel J. Repeta**[2]

[1]Daniel K. Inouye Center for Microbial Oceanography: Research and Education, University of Hawai'i at Mānoa, Honolulu, Hawai'i

[2]Department of Marine Chemistry and Geochemistry, Woods Hole Oceanographic Institution, Woods Hole, Massachusetts

[3]Department of Biology, University of Puget Sound, Tacoma, Washington

## *Abstract*

In oligotrophic ocean regions, dissolved organic phosphorus (DOP) plays a prominent role as a source of phosphorus (P) to microorganisms. An important bioavailable component of DOP is phosphonates, organophosphorus compounds with a carbon-phosphorus (C-P) bond, which are ubiquitous in high molecular weight dissolved organic matter (HMWDOM). In addition to being a source of P, the degradation of phosphonates by the bacterial C-P lyase enzymatic pathway causes the release of trace hydrocarbon gases relevant to climate and atmospheric chemistry. In this study, we investigated the roles of phosphate and phosphonate cycling in the production of methane ($CH_4$) and ethylene ($C_2H_4$) in the western North Atlantic Ocean, a region that features a transition in phosphate concentrations from coastal to open ocean waters. We observed an inverse relationship between phosphate and the saturation state of $CH_4$ and $C_2H_4$ in the water column, and between phosphate and the relative abundance of the C-P lyase marker gene *phnJ*. In phosphate-depleted waters, methylphosphonate and 2-hydroxyethylphosphonate, the C-P lyase substrates that yield $CH_4$ and $C_2H_4$, respectively, were readily degraded in proportions consistent with their abundance and bioavailability in HMWDOM and with the concentrations of $CH_4$ and $C_2H_4$ in the water column. We conclude that phosphonate degradation through the C-P lyase pathway is an important source and a common production pathway of $CH_4$ and $C_2H_4$ in the phosphate-depleted surface waters of the western North Atlantic Ocean and that phosphate concentration can be an important control on the saturation state of these gases in the upper ocean.

Phosphorus (P) is most readily assimilated by microorganisms as inorganic phosphate ($PO_4^{3-}$, hereafter Pi). However, in the stratified surface waters of tropical and subtropical oceans, Pi often occurs at low or limiting concentrations (Wu et al. 2000; Cavendar-Bares et al. 2001; Krom et al. 2010; Moore et al. 2013). In response, microorganisms metabolize bioavailable forms of dissolved organic phosphorus (DOP) to meet their phosphorus (P) requirements (Björkman and Karl 2003; Dyhrman et al. 2007; Lomas et al. 2010). Phosphonates, reduced organophosphorus compounds (P oxidation state of +3) characterized by a C-P bond, are naturally occurring in the high molecular weight fraction of dissolved organic matter (HMWDOM) (Kolowith et al. 2001; Young and Ingall 2010; Repeta et al. 2016) and are potentially a major component of the bioavailable P in the ocean (Clark and Ingall 1998; Repeta et al. 2016), thereby supporting an active P redox cycle in the sea (Karl 2014).

Two phosphonates, methylphosphonate (MPn) and 2-hydroxyethylphosphonate (2-HEP), account for ~ 20% of the P associated with HMWDOM and occur in the form of esters bound to polysaccharides (Repeta et al. 2016). Among marine microorganisms, the marine Thaumarchaeota, *Nitrosopumilus maritimus*, can synthesize MPn, although the cellular function of these phosphonates is unknown (Metcalf et al. 2012). The key enzyme for MPn biosynthesis, MPn synthase, also occurs in the *Pelagibacter* clade of *Alphaproteobacteria*, an abundant member of marine bacterial communities, making this group another likely source of MPn in the ocean (Metcalf et al. 2012; Born et al. 2017). In turn, 2-HEP is an intermediate in the biosynthesis of several phosphonates, including MPn (Shao et al. 2008; Metcalf et al. 2012), and given its prevalence in

*Correspondence: ososa@pugetsound.edu



Additional Supporting Information may be found in the online version of this article.

HMWDOM, it must be synthesized by one or more highly abundant groups of marine microorganisms.

Microbial pathways specialized in C-P bond cleavage are also widespread in the marine environment (Villarreal-Chiu et al. 2012). The C-P lyase pathway is a multiprotein enzyme complex typically expressed under Pi starvation conditions to metabolize phosphonates (White and Metcalf 2007). Recent studies have shown that under Pi stress, bacteria possessing the C-P lyase pathway can utilize the MPn and 2-HEP polysaccharide esters found in HMWDOM to obtain Pi while releasing methane ($CH_4$) and ethylene ($C_2H_4$), respectively, as by-product (Repeta et al. 2016; Sosa et al. 2017). Among marine bacteria, some of the most abundant taxa such as the *Pelagibacter* and *Roseobacter* clades of *Alphaproteobacteria* have acquired C-P lyase and have been shown to degrade phos-phonates (Carini et al. 2014; Sosa et al. 2017). The implication of C-P lyase in methanogenesis via MPn metabolism led to the hypothesis first proposed by Karl et al. (2008) that MPn cycling could explain the so-called ocean "methane paradox" (Kiene 1991), whereby in situ $CH_4$ production occurs in the oxygenated waters of the surface ocean causing supersaturation with respect to atmospheric equilibrium (Lamontagne et al. 1973; Scranton and Brewer 1977; Scranton and Farrington 1977). The ocean is also considered a source of $C_2H_4$ where it is found supersaturated in marine surface waters (Seifert et al. 1999). The degradation of 2-HEP by C-P lyase is potentially an important source of $C_2H_4$ in the ocean (Repeta et al. 2016).

Several additional sources of $CH_4$ have been identified in the ocean (Reeburgh 2007). Among these, anaerobic methanogenic pathways associated with microorganisms inhabiting the oxygen-depleted gut microenvironment of some zooplankton or zooplankton fecal pellets (Marty 1993; de Angelis and Lee 1994; Karl and Tilbrook 1994) were first proposed to support the ocean "methane paradox." Methyl-sulfur metabolism associated with marine algae (Lenhart et al. 2015) and the degradation of dimethylsulfoniopropionate (DMPS), a common osmolyte, and the DMPS degradation product, dimethylsulfide, by heterotrophic bacteria (Damm et al. 2009; Florez-Leiva et al. 2013) have also been reported as possible methanogenic pathways in the ocean. Methane of geological origin can also influence $CH_4$ concentrations in marine systems, particularly in shallow coastal waters (Hovland et al. 1993; Weber et al. 2019).

Previous metagenomic studies have shown that the C-P lyase pathway is most prevalent in ocean regions where Pi is highly depleted such as in surface waters near Bermuda in the Sargasso Sea (Coleman and Chisholm 2010; Martinez et al. 2010). The enrichment of C-P lyase in marine bacterial communities in Pi-depleted environments extends to broader areas of the subtropical North Atlantic Ocean and to the oligotrophic waters in the Mediterranean Sea (Sosa et al. 2019). In these regions, Pi scarcity can limit bacterial growth and productivity (Cotner et al. 1997; Van Wambeke et al. 2002; Obernosterer et al. 2003; Thingstad et al. 2005), and, therefore, the degradation of phosphonates must be an important mechanism to acquire P. Collectively, these observations indicate that degradation of HMWDOM phosphonates through C-P lyase, particularly in Pi-depleted marine environments, may lead to enhanced production of $CH_4$ and $C_2H_4$ in the upper ocean.

In this study, we investigated the cycling of phosphonates across a Pi transition in the western North Atlantic Ocean. We quantified MPn and 2-HEP in HMWDOM, evaluated the relationship between the concentrations of dissolved $CH_4$ and $C_2H_4$ and the concentration of Pi in the upper ocean, tested the potential for phosphonate degradation in surface waters by natural microbial assemblages, and quantified the abundance of C-P lyase in bacterial communities. Through this multifaceted approach, we evaluate if phosphonates can support $CH_4$ and $C_2H_4$ supersaturation in the region and the role of Pi concentration in controlling phosphonate turnover and the production of $CH_4$ and $C_2H_4$ in the upper ocean.

## Materials and methods

### Water column profiles and seawater sampling

Samples were collected on the *Phosphorus*, *Hydrocarbons*, *And Trichodesmium (PHAT)* oceanographic research cruise on board the R/V *Neil Armstrong* (AR16) in May 2017 (Fig. 1). A rosette sampler equipped with conductivity-temperature-depth (CTD) sensors (Sea-Bird Scientific) and 20-liter Niskin® bottles was used to acquire salinity, temperature, density, and chlorophyll fluorescence profiles, and to collect seawater samples for nutrient and hydrocarbon gas concentration determinations at each site. Buoyancy (Brunt–Väisälä) frequency ($N$) was calculated from CTD profile data using the Gibbs-seawater oceanographic toolbox TEOS-10 equation. The cruise map (Fig. 1) was created with the marmap package for R (Pante and Simon-Bouhet 2013). Latitudinal sections of hydrography and biogeochemical measurements were plotted in Ocean Data View version 5.1.5 (Schlitzer 2018) with weighted-average gridding and linear color scale mapping. A conservative gridding scale-length setting produced white spaces between distantly located sampling sites in section plots. The section plots corresponding to the AR16 cruise were constrained with data collected from near-surface waters to 1000 m depth.

### Nutrient analyses

Seawater samples for nutrient analyses were stored frozen (−20°C) in acid-cleaned, high-density polyethylene bottles immediately after collection. Pi concentrations were measured using the modified molybdenum-blue Murphy-Riley method on an AutoAnalyzer 3 High Resolution (Seal Analytical) system as described previously (Foreman et al. 2019). Accuracy was determined by daily measurements of the Wako CSK standard Pi solution at 0.5 $\mu$mol $L^{-1}$ (Wako #034-10011). An average value of $0.499 \pm 0.005$ ($1\sigma$) $\mu$mol $L^{-1}$ P was obtained for

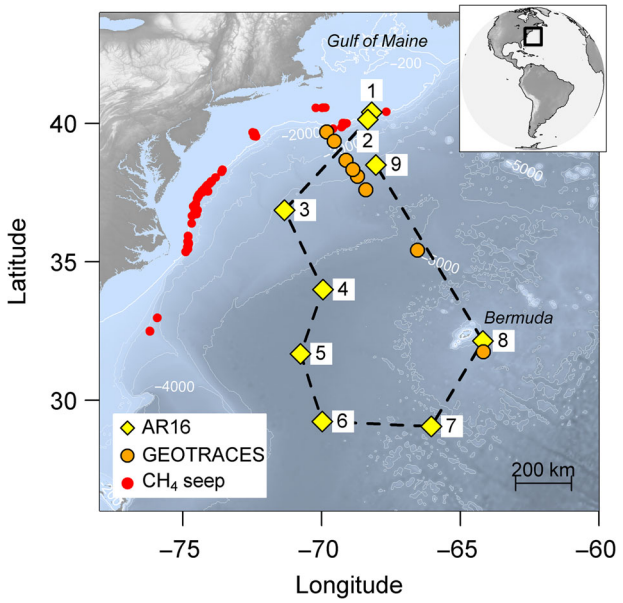


**Fig 1** Regional map of the western North Atlantic Ocean indicating the AR16 cruise sampling sites. The AR16 cruise sampling stations are indicated by yellow diamonds and are numbered 1–9. The sampling locations of GEOTRACES metagenomes representative of the region sampled during cruise AR16 are indicated by orange circles. The locations of $CH_4$ seeps identified in the New England shelf and along the continental margin (Skarke et al. 2014) are indicated by red circles. Isobaths are indicated by white contour lines and are labeled based on their depth relative to sea level in meters. The region covered by the AR16 cruise is demarcated in the world map inset.

the reference standard. Seawater samples with very low Pi concentrations (< 0.1 $\mu$mol $L^{-1}$) were analyzed using the MAGnesium Induced Co-precipitation (MAGIC) technique (Karl and Tien 1992) with several modifications to increase the sensitivity of Pi detection (Thomson-Bulldis and Karl 1998; Cavendar-Bares et al. 2001). Briefly, 150 mL of whole seawater was dispensed into three separate 50 mL conical tubes in equal volumes. To concentrate Pi by MAGIC, 0.25 mL of 1 mol $L^{-1}$ NaOH was added to each tube (0.5% v/v addition) and the tubes were centrifuged at 1000 × $g$ for 1 h. The supernatant was aspirated and the magnesium hydroxide pellets were dissolved in 1.75 mL of 0.1 mol $L^{-1}$ HCl, and combined. Samples were treated with 0.6 mL of arsenate reducing solution (containing 22.4 mmol $L^{-1}$ sodium thiosulfate as the reducing agent) for 15 min to remove arsenate interference and with 0.6 mL of molybdenum blue mix for 1 h to develop color. Pi standards were prepared with Pi-depleted MAGIC supernatant of Sargasso Sea surface seawater collected during the cruise. After Pi addition, standards were treated in the same manner as samples. Standard and sample light absorbance at 880 nm was determined in a 10-cm pathlength cell with a Beckman DU 640 spectrophotometer. The limits of detection (LOD) and quantification (LOQ) of Pi in the MAGIC assay were 0.4 nmol $L^{-1}$ and 0.7 nmol $L^{-1}$, respectively, based on measurements of Pi concentration in the MAGIC-treated Sargasso Sea surface seawater which served as the blank value for the assay.

Total dissolved phosphorus (TDP) concentrations in seawater were measured by a photo-oxidation procedure in which controlled exposure to ultraviolet radiation converts organic P to Pi which is then measured by the modified molybdenum blue method adapted for the auto-analyzer (Foreman et al. 2019). DOP was calculated as the difference between TDP determined by photo-oxidation and Pi determined by MAGIC or by the auto-analyzer method. Because the arsenate reducing procedure was not included in this analysis, phosphite, arsenite, or dissolved organic arsenic (both +5 and +3 As oxidation states), if present, would be included in the estimation of DOP concentrations reported herein. The reproducibility of DOP determinations was ± 5 nmol $L^{-1}$ (1$\sigma$) based on measurements of a reference seawater sample over multiple days.

Inorganic nitrogen (N) concentrations were measured as the sum of nitrate plus nitrite (N + N) by the auto-analyzer method as described previously (Foreman et al. 2019). Seawater samples with very low N + N concentrations (< 20 nmol $L^{-1}$) were measured using the chemiluminescent method based on titanium (III) trichloride reduction of N + N to nitric oxide gas and detection with an Antek model 7090 as described previously (Foreman et al. 2016). The chemiluminescent method had a LOD of 1 nmol $L^{-1}$ N. Accuracy was determined by daily measurements of the Wako CSK standard nitrate solution at 40.0 $\mu$mol $L^{-1}$ N (Wako #037-10241) and 5.0 $\mu$mol $L^{-1}$ N (Wako #036-10191). Average values of 39.21 ± 0.60 (1$\sigma$) $\mu$mol $L^{-1}$ N and 5.04 ± 0.05 (1$\sigma$) $\mu$mol $L^{-1}$ N were obtained for the two reference standards, respectively.

### Sampling, elemental analysis, and $^{31}$P-nuclear magnetic resonance analysis of HMWDOM

Surface seawater (700 L) was drawn from the ship's clean seawater sampling system. Samples were filtered (0.2 $\mu$m) inline and the high molecular weight fraction concentrated using a cross-flow ultrafiltration system fitted with a GE/Osmonics GE series membrane. The membrane has a pore size of ~ 1 nm and nominally retains organic matter of MW > 1 kDa (laboratory tests showed > 99% retention of vitamin $B_{12}$ [MW 1250]). Samples were concentrated to 15–20 L, frozen, and returned to shore for further processing. In the laboratory, concentrates were reduced in volume to 2 L by bench-top ultrafiltration, desalted by serial (~ 10x; 2 L each) dilution/concentration with ultrahigh purity water, and filtered through an Ultracel 30 kDa membrane (Millipore) to remove viruses and other small particles. Samples were subsequently freeze-dried to a fluffy white powder. The total C and N content of HMWDOM was determined by combustion of the powder on a CE-440 Elemental Analyzer (Exeter Analytical). The protocol yielded a final product that was 20–34% of total dissolved organic carbon (DOC), 31–38% by weight C, with a C : N molar ratio of ~ 14. For determination of the total P

content of HMWDOM samples, a known mass of freeze-dried HMWDOM was dissolved in surface seawater previously collected from oligotrophic Hawaiian waters and TDP was measured by the UV photo-oxidation method (Foreman et al. 2019). The TDP concentration in the background low nutrient seawater was subtracted to obtain the P concentration contributed by HMWDOM.

Nuclear magnetic resonance (NMR) spectra were acquired at 25°C in 100% $D_2O$ on a Bruker 400 AVANCE spectrometer 400-DPX (162 MHz for $^{31}P$) fitted with a 5 mm inverse broadband probe and running TOPSPIN 1.3. Phosphorus chemical shifts ($\delta$) are reported relative to 85% phosphoric acid ($\delta$ = 0 ppm). For proton-decoupled $^{31}P$ spectra, we used "zgdc30" with WALTZ16 decoupling and a 10 s relaxation delay, > 100,000 scans, and 15 Hz line broadening. To determine the ratio of MPn to 2-HEP in our samples, ~ 10 mg of HMWDOM was dissolved in 1 mL of 2 mol $L^{-1}$ KOH and heated at 80°C for 24 h. This treatment hydrolyzes phosphonate-polysaccharide esters in HMWDOM, which otherwise appear as broad peaks that are not fully resolved in the $^{31}P$ NMR spectrum. Free phosphonates appear as sharp, well-resolved signals that can be more readily integrated. The sample was diluted 10x with ultrahigh purity water, treated with AG 50W-8X cation exchange resin until the pH was slightly acidic (~ 4 h), then filtered and freeze-dried. The dry sample was dissolved in 100% $D_2O$ and the $^{31}P$ NMR spectra recorded.

### Dissolved $CH_4$ and $C_2H_4$ concentration measurements

Seawater for $CH_4$ and $C_2H_4$ concentration measurements was siphoned gently from the rosette sampling bottles into the bottom of combusted 200-mL glass serum bottles. Bottles were allowed to overflow with an equivalent of three volumes of seawater before poisoning with 0.1 mL of saturated mercuric chloride solution (7% w/v) and sealing with polytetrafluoroethylene-lined stoppers and aluminum crimp collars. Samples were stored at ambient temperature in the dark until gas chromatographic analysis aboard the ship, typically within 4 h after sampling.

Dissolved $CH_4$ and $C_2H_4$ concentrations were measured with an Agilent 7980A gas chromatograph equipped with a flame ionization detector (FID) and a gas stripping and cryo-trap as described previously (Wilson et al. 2017). The FID was calibrated daily by injecting different volume sized loops of a gaseous standard containing 10 ppm of $CH_4$ and $C_2H_4$ in pure nitrogen gas (Scott-Marrin). Dissolved gases were stripped from 200 mL seawater samples with ultrahigh purity helium for 12 min and concentrated onto a Porapack Q® trap (80–100 sieve mesh size) cooled in liquid nitrogen. The helium was further purified prior to use in the sample transfer and sparging process by passage through an additional liquid nitrogen cryo-trap. All peaks corresponding to $CH_4$ and $C_2H_4$ were manually selected and integrated on the Agilent ChemStation software. The LOD and LOQ for $CH_4$ (23.6 pmol and 71.9 pmol, respectively) and $C_2H_4$ (4.6 pmol and 14.0 pmol, respectively) were calculated based on the root mean square error (RMSE) of the gas standard calibration, where LOD = 3.29 RMSE, and LOQ = 10 RMSE (Bernal 2014). The LOD and LOQ corresponded to seawater $CH_4$ concentrations of 130 pmol $L^{-1}$ and 380 pmol $L^{-1}$, respectively, and $C_2H_4$ concentrations of 25 pmol $L^{-1}$ and 75 pmol $L^{-1}$, respectively.

### Methane and ethylene saturation and sea–air flux calculations

The extent to which the measured $CH_4$ and $C_2H_4$ concentrations in seawater ($C_{meas}$) deviated from the predicted atmospheric equilibrium solubility concentrations ($C_{eq}$) was expressed as the molar differences ($C_{meas} - C_{eq}$) $\Delta CH_4$ and $\Delta C_2H_4$, respectively. This deviation was also expressed as the percent saturation level, where 100% corresponds to $\Delta CH_4 = 0$ or $\Delta C_2H_4 = 0$. Equilibrium concentrations of $CH_4$ in seawater were calculated based on the Bunsen solubility equation of Wiesenburg and Guinasso (1979) using measured temperature and salinity, and an atmospheric $CH_4$ concentration of 1905.6 ppb (Tudor Hill, Bermuda monthly average for 2017) obtained from the National Oceanic and Atmospheric Administration Earth System Research Laboratory (NOAA-ESRL) Global Monitoring Division. Equilibrium concentrations of $C_2H_4$ in seawater were calculated based on the Bunsen solubility equation of Breitbarth et al. (2004) using measured temperature and salinity, and an average atmospheric $C_2H_4$ concentration of 0.4 ppb based on values reported over the North Atlantic Ocean (Rudolph and Ehhalt 1981). $CH_4$ and $C_2H_4$ sea–air flux estimates ($F$) were calculated with the equation:

$$F = k\left(C_{meas} - C_{eq}\right)$$

where $k$ is the gas transfer coefficient obtained from the wind speed parameterization by Wanninkhof (2014) and ($C_{meas} - C_{eq}$) is the average $\Delta CH_4$ or $\Delta C_2H_4$ concentration in the surface mixed layer. For $C_2H_4$ flux calculations, the $C_2H_4$-specific Schmidt number for the Wanninkhof (2014) parameterization was calculated with the diffusion coefficient equations implemented in the Johnson (2010) module for R software. Daily advanced scatterometer (ASCAT) gridded surface wind speed fields adjusted to 10 m above sea level (Bentamy and Croize Fillon 2012) were produced by the Centre ERS d'Archivage et de Traitement (CERSAT), at IFREMER, Plouzané (France) and were downloaded from the Asia-Pacific Data Research Center in the School of Ocean and Earth Science at the University of Hawai'i at Mānoa. Average wind speeds of the week prior to sampling in an area comprising ± 0.25° latitude and longitude over the sampling location were used as input in the $k$ parameterization. The depth of the surface mixed layer was calculated from seawater density profiles and a density criterion of 0.125 kg $m^{-3}$ from the surface (Kara et al. 2000). The sea–air flux was calculated only at stations where at least one depth within the surface mixed layer

was sampled for $CH_4$ and $C_2H_4$ concentration measurements. Positive sea–air fluxes indicated that the ocean is a source of atmospheric $CH_4$ or $C_2H_4$.

**Seawater incubation experiments**

To compare the phosphonate degradation potential of microbial communities along the cruise transect, near-surface seawater was amended with combinations of inorganic N ($NO_3^- + NH_4^+$), glucose as a source of carbon, and MPn and 2-HEP as a source of P. Inorganic N was supplied as 28 $\mu$mol $L^{-1}$ $NaNO_3$ (99.0% purity, Sigma-Aldrich) plus 4 $\mu$mol $L^{-1}$ $NH_4Cl$ (≥ 99.99% purity, Fluka). D-glucose (≥ 99.5% purity, Sigma-Aldrich) was supplied at a concentration of 33.3 $\mu$mol $L^{-1}$. MPn (98% purity, Alfa Aesar) and 2-HEP (95% purity, BOC Sciences) were provided at concentrations of 0.1 $\mu$mol $L^{-1}$. C, N, and P additions resulted in a C : N molar ratio of 6.25, close to published values of marine bacteria, and a C : P molar ratio much higher than values reported for marine bacteria (Goldman et al. 1987; Gundersen et al. 2002). The relatively low added P prevented excessive metabolic activity leading to oxygen depletion and was sufficient to stimulate growth and gas production. Samples were incubated 4–8 d in gas-tight glass serum bottles at in situ temperature in the dark to measure the net production of $CH_4$ and $C_2H_4$ by gas chromatography. To test if the $CH_4$ and $C_2H_4$ produced in seawater samples amended with inorganic N, phosphonates, and/or glucose was significantly greater than in control samples supplied only with inorganic N, a one-tailed Student's *t*-test was applied and evaluated at a 0.05 significance level.

**Bioavailability of HMWDOM phosphonates**

The C-P lyase-containing bacterium *Pseudomonas stutzeri* strain HI00D01 was used to test the bioavailability of MPn and 2-HEP contained in Sargasso Sea HMWDOM as described previously (Repeta et al. 2016). Purified HMWDOM (collected at Sta. 5) was added at a concentration of ~ 3.3 $\mu$g $mL^{-1}$ to morpholinopropanesulfonic acid (MOPS) minimal medium containing glucose (33.3 $\mu$mol $L^{-1}$) for the growth of *P. stutzeri*. HMWDOM-enriched medium was inoculated with *P. stutzeri* cells pregrown in MOPS minimal medium (containing 9.5 mmol $L^{-1}$ $NH_4Cl$) depleted of Pi and incubated in gas-tight glass bottles at 22°C. The $CH_4$ and $C_2H_4$ produced during culture growth were measured by gas chromatography as described for field samples.

**Statistical analyses**

To evaluate the overall relationship between $\Delta CH_4$ and $\Delta C_2H_4$ concentrations and the environmental parameters measured in the cruise transect, simple linear regression models were calculated. The overall significance of the regression models was tested with the *F*-test at a 0.05 significance level. To evaluate the relationships between buoyancy frequency (*N*), chlorophyll fluorescence, $\Delta CH_4$, and $\Delta C_2H_4$ in each sampling site, we calculated Pearson correlation coefficients and tested their significance at a 0.05 significance level. To obtain values of *N* that corresponded to the depths of $CH_4$ and $C_2H_4$ discrete measurements, the depth profiles of *N* were binned into 10 m intervals and the means of each bin were linearly interpolated to produce a depth-dependent predictor function. To obtain values of chlorophyll fluorescence that corresponded to the depths of $CH_4$ and $C_2H_4$ discrete measurements, the depth profiles of chlorophyll fluorescence were binned into 5 m intervals and the means of each bin were linearly interpolated to produce a depth-dependent predictor function.

**Metagenomic analysis of C-P lyase abundance**

To quantify the abundance of the C-P lyase pathway in microbial communities, we focused on the gene *phnJ*, which encodes the key enzyme that catalyzes C-P bond cleavage and has been shown to be a good marker for its presence (Sosa et al. 2019). We examined *phnJ* in 46 metagenomes obtained during the US GEOTRACES program Section GA03 representative of the region sampled during the AR16 cruise in the western North Atlantic Ocean (Fig. 1). One important caveat is that the GEOTRACES metagenomes analyzed were sampled in November 2011 while cruise AR16 took place in May 2017, and it is well recognized that the western North Atlantic Ocean exhibits significant annual environmental variability. Metagenomic assemblies were downloaded from the iMicrobe database (https://www.imicrobe.us/#/projects/277) and raw paired-end reads were obtained from the NCBI Sequence Read Archive. Metagenome sample names, SRA accessions, and metadata are provided in the Supporting Information Table S1 as described by Biller et al. (2018). Prodigal (Hyatt et al. 2010) was implemented to identify coding DNA sequences (CDS) in the assemblies. Paired-end reads were quality-trimmed with Trimmomatic (Bolger et al. 2014) as described by Biller et al. (2018). Trimmed reads were mapped to the assemblies with Bowtie2 (Langmead and Salzberg 2012). Coverage for all predicted CDS was determined with the Bedtools (v.2.27.1) coverage tool (Quinlan and Hall 2010). To identify *phnJ* genes, we built a profile hidden Markov model of C-P lyase protein PhnJ with HMMER v.3.1b2 (Eddy 2009) using a multiple sequence alignment of curated C-P lyase amino acid sequences from the marine environment (Sosa et al. 2019). The profile was used to search for CDS in the metagenomic assembly matching PhnJ with an E-value of ≤ 0.001. To calculate the abundance of C-P lyase in each metagenome, the coverage of C-P lyase *phnJ* genes identified with HMMER was summed and normalized by the coverage of 40 universal single-copy genes. Single-copy genes were identified with the fetchMGs tool (Sunagawa et al. 2013). More specifically, in each metagenome, the coverage of all CDS matching each single-copy gene was summed and the median of the summed coverage of the 40 single-copy genes was used to normalize *phnJ* coverage. This calculation provided an estimate of the percentage of organisms that possess C-P lyase and assumed there was

one copy of *phnJ* per organism. CTD temperature and seawater nutrient concentration measurements corresponding to the GEOTRACES Section GA03 were downloaded from the GEOTRACES Intermediate Data Product 2017 database (Schlitzer et al. 2018).

## Results

### Water column characteristics

Surface temperature was ~ 7°C on the New England shelf, 14–17°C within the shelf break, where the seafloor transitions to the continental slope, and the Gulf Stream, and 21–24°C south of the Gulf Stream in the Sargasso Sea region (Fig. 2a). Seawater density in the surface mixed layer was lowest immediately south of the Gulf Stream in Sta. 3, highest in waters near the shelf break and north of the Gulf Stream, and intermediate during the remainder of the cruise. The depth of the surface mixed layer also varied along the cruise track. In the shelf region, the surface mixed layer was 30 m deep, and near the shelf break it deepened to 40 m. The shallowest surface mixed layer (12 m) occurred at Sta. 9, located slightly north of the Gulf Stream. South of the Gulf Stream, the surface mixed layer depth (MLD) ranged from 27 to 55 m except at Sta. 6 where the surface mixed layer was 14 m deep.

### Phosphorus and nitrogen nutrient distributions

Nutrient concentrations were consistent with those observed in a previous transect in the western North Atlantic Ocean during March 1998 (Cavendar-Bares et al. 2001). Surface Pi concentrations were highest in the region north of the Gulf Stream, 550 nmol $L^{-1}$ in shelf waters (Sta. 1), declined to 150 nmol $L^{-1}$ near the shelf break (Sta. 2), and reached 1–8 nmol $L^{-1}$ in Sta. 3–8 south of the Gulf Stream in the Sargasso Sea (Fig. 2b). Surface N + N concentrations followed a similar trend as Pi. N + N was highest in the region north of the Gulf Stream reaching 2.7 $\mu$mol $L^{-1}$ in shelf waters and 0.86 $\mu$mol $L^{-1}$ near the shelf break. South of the Gulf Stream, surface N + N dropped considerably and ranged from 1 to

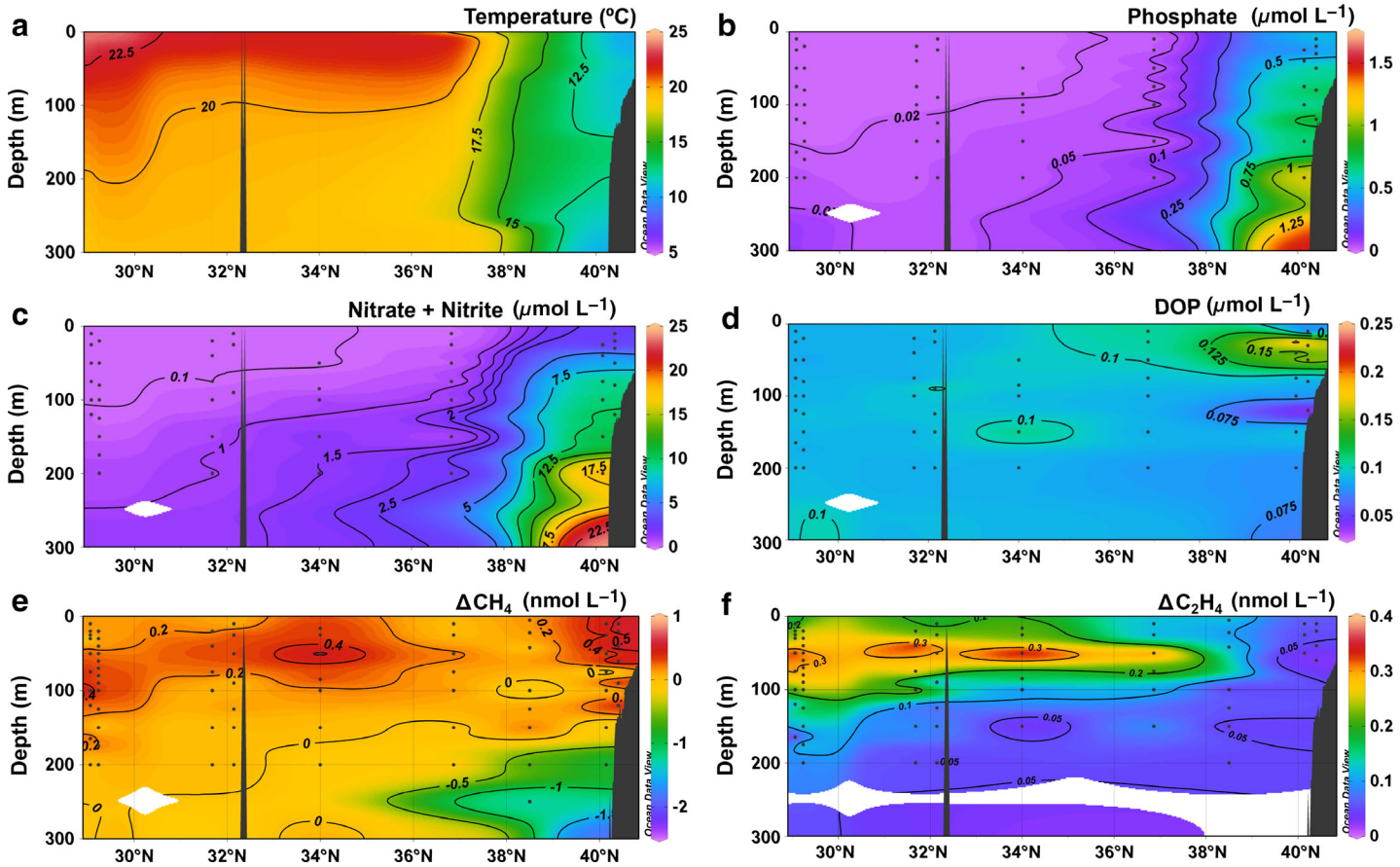


**Fig 2** Latitudinal sections of temperature, dissolved nutrients, and methane and ethylene saturation. The gray symbols indicate the latitude and depth of discrete samples. The contours represent regions with equal parameter values. For geographic reference, the bathymetry along the continental margin and Bermuda (latitude 32.3°N) is represented as black shading. (**a**) Temperature (°C). (**b**) Inorganic phosphate concentration ($\mu$mol $L^{-1}$). (**c**) Inorganic nitrate plus nitrite (N + N) concentration ($\mu$mol $L^{-1}$). (**d**) DOP concentration ($\mu$mol $L^{-1}$). (**e**) Section depicting the difference between the measured concentration of methane ($CH_4$) and the concentration predicted at solubility equilibrium with the atmosphere ($\Delta CH_4$), where $\Delta CH_4 > 0$ nmol $L^{-1}$ indicates supersaturation and $\Delta CH_4 < 0$ nmol $L^{-1}$ indicates undersaturation. (**f**) The corresponding section of ethylene ($C_2H_4$), where $\Delta C_2H_4 > 0$ nmol $L^{-1}$ indicates supersaturation.

17 nmol $L^{-1}$ (Fig. 2c). Surface DOP was lowest in shelf waters, only 28 nmol $L^{-1}$, increased to 220 nmol $L^{-1}$ near the shelf break, and ranged from 84 to 105 nmol $L^{-1}$ south of the Gulf Stream in the Sargasso Sea (Fig. 2d).

The vertical distributions of nutrients also varied across sampling sites (Fig. 2). In shelf waters (Sta. 1), N + N and Pi reached 10.4 $\mu$mol $L^{-1}$ and 0.82 $\mu$mol $L^{-1}$, respectively, at 120 m depth. Near the shelf break (Sta. 2), N + N and Pi increased to 8 $\mu$mol $L^{-1}$ and 0.5 $\mu$mol $L^{-1}$, respectively, near the base of the surface mixed layer (40 m depth). South of the Gulf Stream (Sta. 3–8), N + N concentrations of < 1 $\mu$mol $L^{-1}$ and Pi concentrations of < 0.1 $\mu$mol $L^{-1}$ occurred in the upper 200 m. In turn, a maximum in DOP concentration of approximately 170 nmol $L^{-1}$ occurred in shelf waters between 30 and 50 m. In waters past the shelf break, DOP declined steadily from maximum values in the surface to near constant values of 71–76 nmol $L^{-1}$ from 200 to 1000 m. In sites south of the Gulf Stream, DOP typically varied between 80 and 90 nmol $L^{-1}$ in the upper 300 m and dropped to 60–70 nmol $L^{-1}$ from this depth to 1000 m.

### Characterization of HMWDOM phosphonates

HMWDOP accounted for 44% of DOP concentrations at Sta. 2 (shelf break), 77% at Sta. 4 (NW Sargasso Sea), and 42% at Sta. 7 (mid-Sargasso Sea) in the surface mixed layer. The C : P ratio of HMWDOM ranged from 270 at Sta. 2, to 290 at Sta. 4, to 346 at Sta. 7. $^{31}$P NMR spectra of HMWDOM from all three stations were very similar, with major signals from phosphonate esters (23% total P; $\delta$ of 20–30 ppm), phosphate esters (69% total P; $\delta$ of −5 to 5 ppm), and pyrophosphate esters (7% total P; $\delta$ of −12 to −5 ppm). Hydrolysis of HMWDOM phosphonate esters from Sargasso Sea surface waters (Sta. 4, 5, 6, 7, and 8) yielded MPn and 2-HEP in an approximately 11:1.1 ± 0.1 (1 σ, $n$ = 5) ratio, along with minor unidentified phosphonates. The change in C : P molar ratio of HMWDOM between stations was not reflected in changes in the distribution of phosphorus functional groups, or the major phosphonates in HMWDOM. Based on P content and $^{31}$P NMR analysis of HMWDOM, phosphonates accounted for 10% of DOP concentrations at Sta. 2, 18% at Sta. 4%, and 10% at Sta. 7 in the surface mixed layer.

### Patterns of $CH_4$ and $C_2H_4$ supersaturation

The depth at which $CH_4$ and $C_2H_4$ concentrations in exceeded atmospheric solubility equilibrium concentrations ($\Delta CH_4$ and $\Delta C_2H_4 > 0$ nmol $L^{-1}$, which indicates supersaturation) varied among sites (Fig. 2e,f). Methane supersaturation was the highest in shelf waters (Sta. 1) ($\Delta CH_4$ = 470–850 pmol $L^{-1}$) where it persisted throughout the water column. Ethylene was supersaturated in shelf waters in the upper 60 m. The concentration of $\Delta C_2H_4$ ranged from 26 to 52 pmol $L^{-1}$ and were on average 20-fold lower than $\Delta CH_4$ concentrations. Near the shelf break (Sta. 2), $CH_4$ was

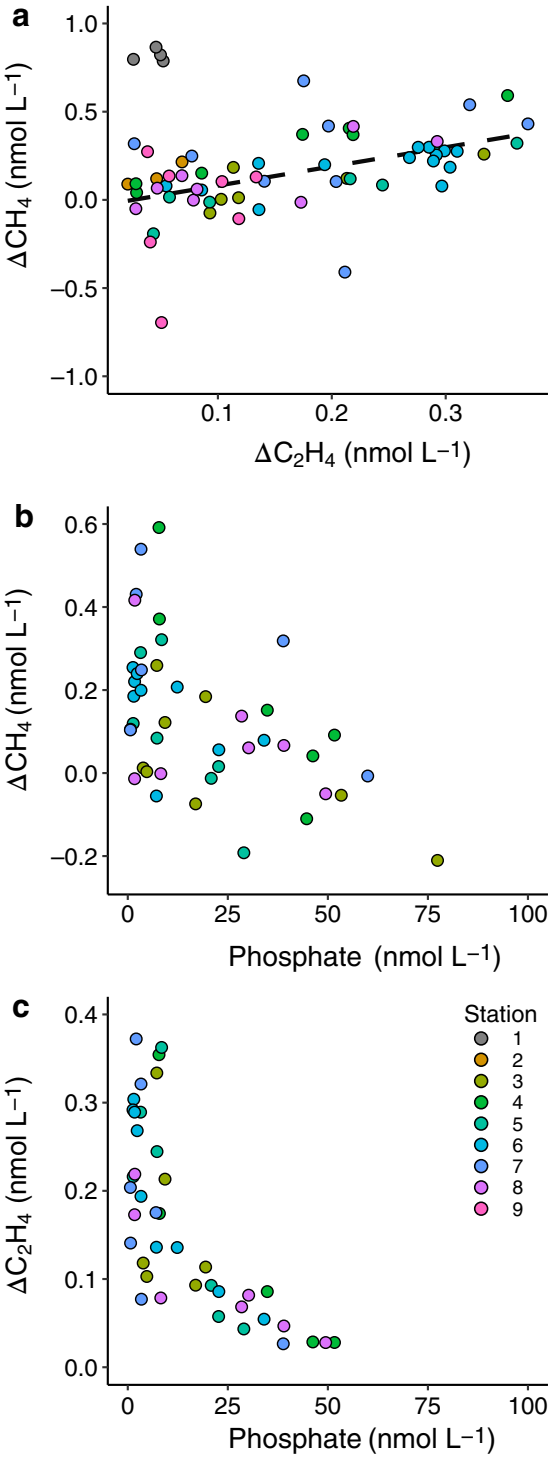


**Fig 3** Methane and ethylene supersaturation with respect to phosphate. (**a**) Relationship between the difference in methane ($\Delta CH_4$) and ethylene ($\Delta C_2H_4$) concentrations with respect to atmospheric equilibrium solubility concentrations. The dashed line represents a linear regression model of $\Delta CH_4$ and $\Delta C_2H_4$ concentrations, excluding data from the New England shelf (Sta. 1). (**b**) Distribution of $\Delta CH_4$ with respect to phosphate (Pi) concentrations in surface waters where Pi < 100 nmol $L^{-1}$. (**c**) Distribution of $\Delta C_2H_4$ with respect to Pi concentrations in surface waters where Pi < 100 nmol $L^{-1}$. Data points are color coded by station number as indicated. The same color code applies to all panels.

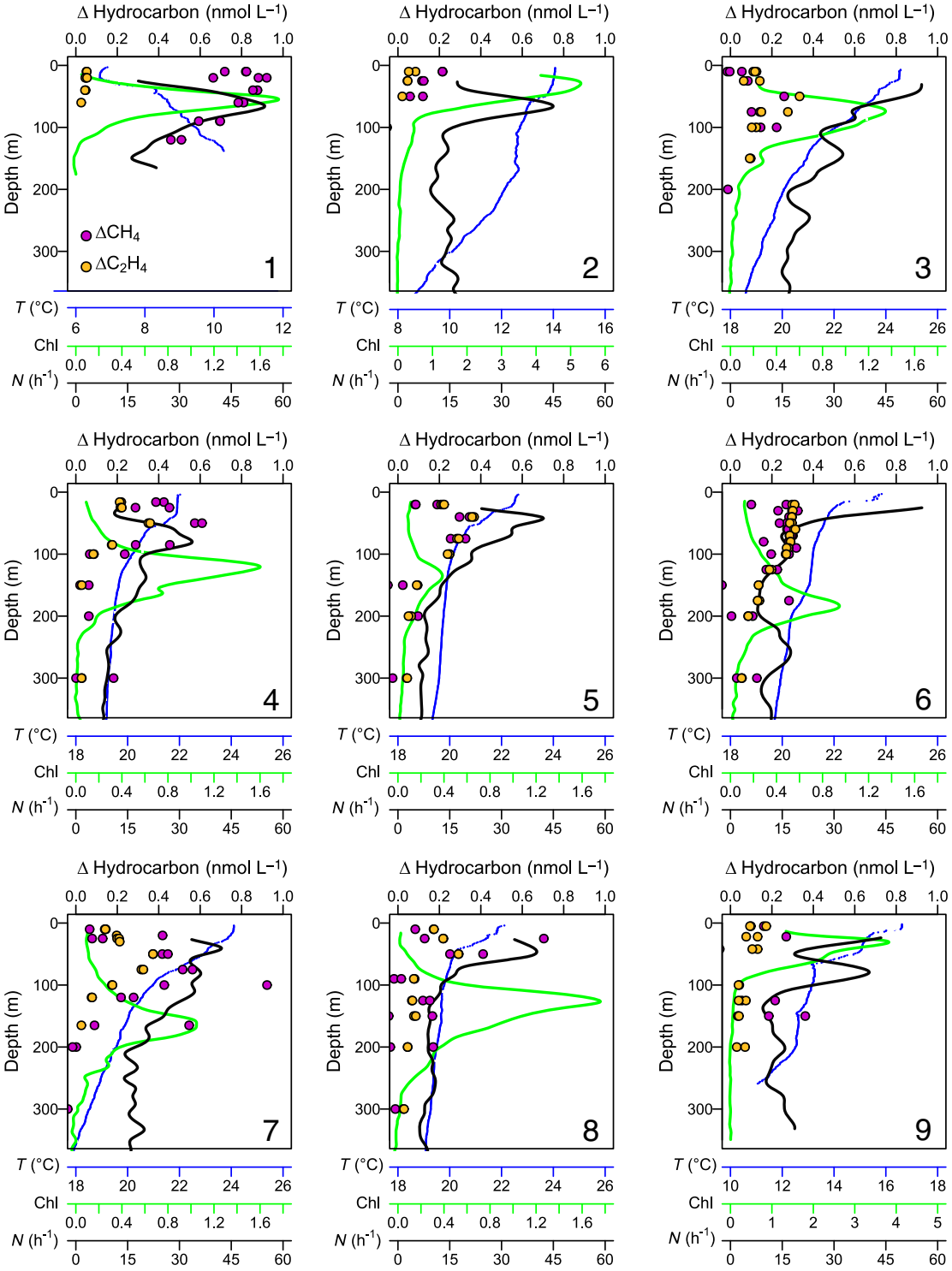


**Fig 4** Water column profiles of methane and ethylene concentration above saturation, temperature, chlorophyll, and buoyancy frequency. The depth profiles depict the difference between measured seawater methane and ethylene concentrations and the predicted atmospheric equilibrium solubility concentrations, $\Delta CH_4$ (magenta symbols) and $\Delta C_2H_4$ (gold symbols), respectively. The panel numbers correspond to the AR16 cruise stations as in Fig. 1. The blue trace corresponds to the CTD temperature (*T*). The green trace corresponds to a model of chlorophyll calculated using 5 m depth intervals of the CTD chlorophyll (Chl) fluorescence signal. In each profile, Chl was scaled with respect to the minimum fluorescent signal detected. The black trace corresponds to a model of buoyancy (Brunt–Väisälä) frequency *N* calculated for 10 m depth intervals.

supersaturated in the upper 50 m ($\Delta CH_4$ = 89–215 pmol $L^{-1}$) and $\Delta C_2H_4$ increased slightly to 21–69 pmol $L^{-1}$ but remained threefold lower than $\Delta CH_4$. North of the Gulf Stream (Sta. 9), at depths where $CH_4$ was supersaturated, $\Delta C_2H_4$ increased further to 57–133 pmol $L^{-1}$, comparable to $\Delta CH_4$ concentrations. In the Sargasso Sea sites, $CH_4$ and $C_2H_4$ supersaturations spanned the upper 150–200 m and at Sta. 6, the upper 300 m. At depths where $CH_4$ was supersaturated, $\Delta C_2H_4$ concentrations (27–372 pmol $L^{-1}$) were comparable to $\Delta CH_4$ concentrations (3–674 pmol $L^{-1}$). Across all sites (excluding Sta. 1), the ratio of $\Delta CH_4$ to $\Delta C_2H_4$ ranged from −14 to 12 (median = 0.97 and mean = 0.92) and their concentrations followed a significant linear relationship ($r^2$ = 0.26, $F_{1,59}$ = 21.7, $p << 0.01$; Fig. 3a).

The linear regression of Pi concentrations and the corresponding $\Delta CH_4$ concentrations from the surface mixed layer to a depth of 1000 m supported an overall significant negative relationship ($r^2$ = 0.79, $F_{1,71}$ = 273, $p << 0.01$). Because N + N and Pi were significantly correlated throughout the region ($r^2$ = 0.96, $F_{1,70}$ = 1579, $p << 0.01$), the trend between Pi and $\Delta CH_4$ was indistinguishable from the relationship between N + N and $\Delta CH_4$ ($r^2$ = 0.86, $F_{1,54}$ = 361, $p << 0.01$). Excluding the shallow shelf waters (Sta. 1), $CH_4$ supersaturation ($\Delta CH_4 > 0$ nmol $L^{-1}$) occurred at depths where the concentration of Pi was less than 50 nmol $L^{-1}$ and increased as Pi concentration decreased below 50 nmol $L^{-1}$ (Fig. 3b). Similarly, $C_2H_4$ supersaturation ($\Delta C_2H_4 > 0$ nmol $L^{-1}$) typically coincided with Pi concentrations of less than 50 nmol $L^{-1}$ and increased as Pi concentrations decreased (Fig. 3c).

The $\Delta CH_4$ and $\Delta C_2H_4$ subsurface maxima in the Sargasso Sea stations were generally situated in the thermocline immediately below the surface mixed layer and above the deep

**Table 1** Correlation analyses of methane and ethylene concentrations with respect to solubility equilibrium ($\Delta CH_4$ and $\Delta C_2H_4$), buoyancy frequency (*N*) and chlorophyll fluorescence (Chl).

| | $\Delta CH_4$, $\Delta C_2H_4$ | | $\Delta CH_4$, *N* | | $\Delta CH_4$, Chl | | $\Delta C_2H_4$, *N* | | $\Delta C_2H_4$, Chl | |
|---|---|---|---|---|---|---|---|---|---|---|
| **Station** | ***R*** | ***p*** | ***R*** | ***p*** | ***R*** | ***p*** | ***R*** | ***p*** | ***R*** | ***p*** |
| 1 | 0.20 | 0.80 | 0.63 | 0.37 | 0.92 | 0.08 | −0.54 | 0.46 | −0.08 | 0.92 |
| 2 | 0.95 | 0.21 | −0.69 | 0.52 | 0.35 | 0.77 | −0.88 | 0.31 | 0.63 | 0.57 |
| 3 | 0.78 | 0.07 | −0.08 | 0.88 | 0.78 | 0.07 | −0.17 | 0.74 | 0.98 | * |
| 4 | 0.99 | * | 0.63 | 0.13 | 0.04 | 0.94 | 0.66 | 0.11 | −0.04 | 0.93 |
| 5 | 0.92 | * | 0.86 | * | 0.31 | 0.50 | 0.94 | * | 0.45 | 0.31 |
| 6 | 0.67 | * | 0.10 | 0.73 | 0.06 | 0.83 | 0.37 | 0.20 | 0.08 | 0.78 |
| 7 | 0.17 | 0.67 | −0.54 | 0.13 | 0.30 | 0.44 | 0.63 | 0.07 | −0.42 | 0.26 |
| 8 | 0.76 | * | 0.59 | 0.13 | −0.25 | 0.55 | 0.68 | 0.06 | −0.25 | 0.56 |
| 9 | 0.25 | 0.59 | 0.33 | 0.47 | 0.25 | 0.59 | 0.88 | * | 0.71 | 0.08 |

Pearson correlation coefficient (*R*) and its corresponding *p* value (*p*).
*Significance was evaluated at the 0.05 level.

**Table 2** Average methane and ethylene concentrations relative to solubility equilibrium ($\Delta CH_4$ and $\Delta C_2H_4$) in the surface mixed layer and sea–air flux estimates.

| **Station** | **Latitude** °N | **Longitude** °W | **MLD (m)** | **$\Delta CH_4$ (pmol $L^{-1}$)** | **$CH_4$ sea–air flux ($\mu$mol $m^{-2}$ $d^{-1}$)** | **$\Delta C_2H_4$ (pmol $L^{-1}$)** | **$C_2H_4$ sea–air flux ($\mu$mol $m^{-2}$ $d^{-1}$)** | **Wind speed (m $s^{-1}$)** |
|---|---|---|---|---|---|---|---|---|
| 1 | 40.40 | 68.19 | 30 | 800 | 1.0 | 50 | 0.1 | 5.5 |
| 2 | 40.14 | 68.33 | 41 | 170 | 0.4 | 60 | 0.1 | 7.0 |
| 3 | 36.86 | 71.34 | 27 | 10 | 0.1 | 110 | 0.9 | 11.1 |
| 4 | 34.00 | 69.95 | 44 | 390 | 1.8 | 220 | 1.0 | 8.7 |
| 5 | 31.68 | 70.76 | 28 | 120 | 0.4 | 220 | 0.7 | 7.4 |
| 6 | 29.23 | 69.97 | 14 | nd | nd | nd | nd | 5.2 |
| 7 | 29.06 | 66.04 | 27 | 210 | 0.6 | 180 | 0.5 | 6.4 |
| 8 | 32.14 | 64.19 | 24 | −10 | 0.0 | 170 | 0.4 | 6.0 |
| 9 | 38.50 | 68.05 | 12 | 130 | 0.5 | 130 | 0.5 | 8.5 |

nd, not determined.

chlorophyll maximum (DCM) (Fig. 4). At depths where $C_2H_4$ was detectable, $\Delta CH_4$ and $\Delta C_2H_4$ concentrations were highly correlated ($p < 0.05$, Pearson; Table 1). The water column below the surface mixed layer was well stratified as indicated by the high values of *N*. The values of $\Delta CH_4$ and $\Delta C_2H_4$ were highly correlated in several Sargasso Sea stations (Table 1). In turn, chlorophyll fluorescence was not significantly correlated to $\Delta CH_4$ or $\Delta C_2H_4$ concentrations, except to $\Delta C_2H_4$ at Sta. 9 (Table 1).

### Estimates of $CH_4$ and $C_2H_4$ sea–air flux

In the region covered by the AR16 cruise, the calculated fluxes of $CH_4$ and $C_2H_4$ from the ocean to the atmosphere ranged from 0.0 to 1.8 $\mu$mol $m^{-2}$ $d^{-1}$ and 0.1 to 1.0 $\mu$mol $m^{-2}$ $d^{-1}$, respectively (Table 2). These estimates are comparable to the range of sea–air fluxes of 0.28–3.98 $\mu$mol $CH_4$ $m^{-2}$ $d^{-1}$ and 0.35–1.16 $\mu$mol $C_2H_4$ $m^{-2}$ $d^{-1}$ in the subtropical Atlantic Ocean reported by Seifert et al. (1999). The highest $CH_4$ sea–air flux occurred at Sta. 4 in the Sargasso Sea west of Bermuda which averaged wind speeds of 8.7 m $s^{-1}$ and featured a 44 m deep surface mixed layer with $\Delta CH_4$ concentrations equivalent to 117–119% saturation. The second highest $CH_4$ sea–air flux occurred at Sta. 1 in shallow New England shelf waters. The highest $C_2H_4$ sea–air flux also occurred at Sta. 4 in the Sargasso Sea and the lowest at Sta. 1 in shelf waters. Ethylene fluxes were generally higher at the

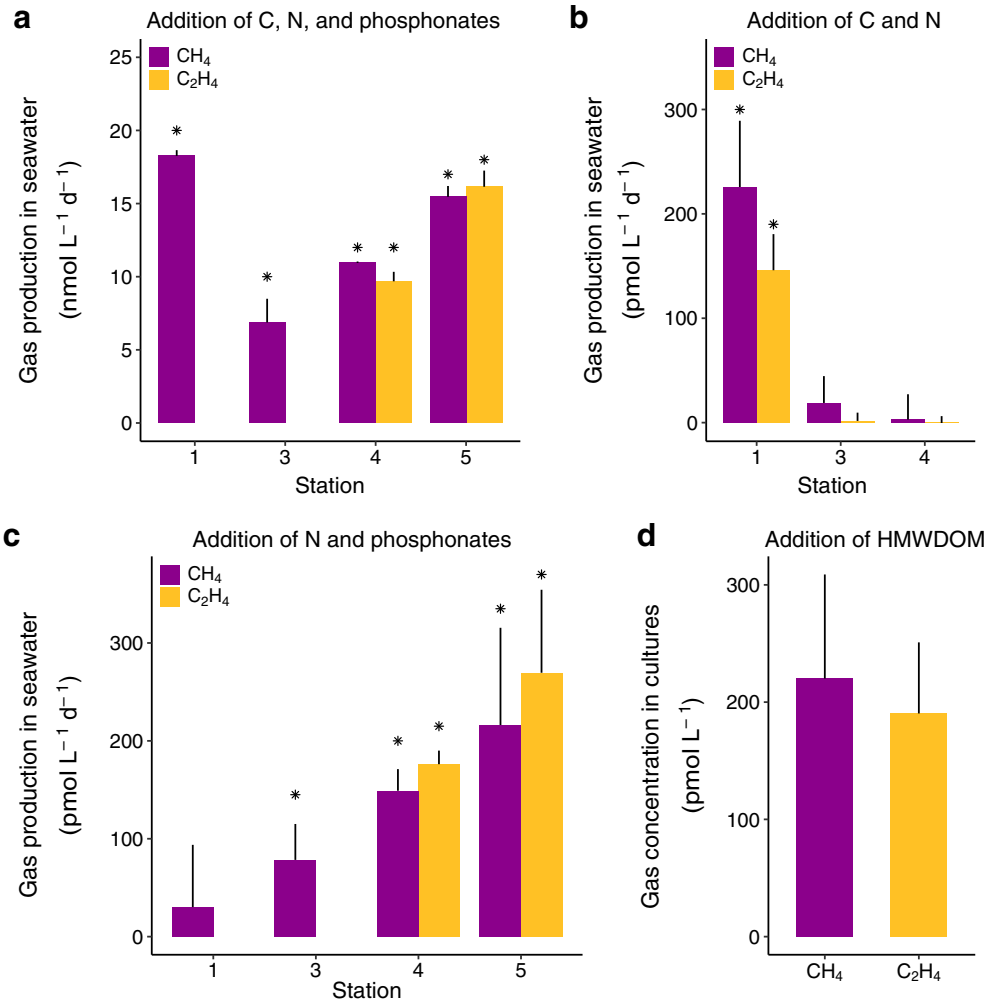


**Fig 5** Degradation potential of MPn and 2-HEP in the western North Atlantic Ocean inferred from the production of methane ($CH_4$) and ethylene ($C_2H_4$). (**a**) Seawater samples amended with inorganic N, glucose, and MPn or 2-HEP. (**b**) Seawater samples amended with glucose and inorganic N (no exogenous phosphonates supplied). (**c**) Seawater samples amended with inorganic N, MPn, and 2-HEP. Samples from Sta. 1 and 3 were only amended with MPn and, therefore, only $CH_4$ concentrations are reported. The data in panels (**a**–**c**) represent the increase in $CH_4$ or $C_2H_4$ in seawater incubation experiments with respect to control samples during cruise AR16 Sta. 1, 3, 4, and 5 (* indicates a significant increase in gas concentration; $p < 0.05$, one-tailed *t*-test). Table 3 describes sample treatments and incubation conditions. The control samples were only supplied with inorganic N (28 $\mu$mol $L^{-1}$ $NaNO_3$ and 4 $\mu$mol $L^{-1}$ $NH_4Cl$). The gas produced was normalized by the incubation period. (**d**) The concentration of $CH_4$ and $C_2H_4$ produced in cultures of the C-P lyase-containing bacterium *P. stutzeri* strain HI00D01 supplied with phosphonate-containing HMWDOM purified from Sargasso Sea surface waters. All experiments were prepared in duplicate. Error bars represent one standard deviation from the mean.

Sargasso Sea stations relative to nearshore waters. In the Sargasso Sea, the $CH_4$ and $C_2H_4$ sea–air fluxes were within a factor of 2 from each other in Sta. 4, 5, and 7. At Sta. 3 and 8, $CH_4$ concentrations in the surface mixed layer were close to equilibrium with the atmosphere and $\Delta C_2H_4$ was higher than $\Delta CH_4$.

### Mass balance between $CH_4$ and $C_2H_4$ sea–air flux and phosphonate turnover

DOC concentrations in surface waters at the time of our sampling were 67–70 $\mu$mol $L^{-1}$. We used the C : P and phosphonate : total phosphorus (measured by $^{31}P$ NMR) ratios of HMWDOM to calculate the phosphonate inventory in the surface mixed layer (Table 2) at the northern flank of the Gulf Stream (Sta. 2: 0.71 mmol $m^{-2}$) and the Sargasso Sea (Sta. 4: 0.77 mmol $m^{-2}$; Sta. 7: 0.24 mmol $m^{-2}$). Assuming that phosphonates are the primary source of $CH_4$ and $C_2H_4$ in the region and that our calculated $CH_4$ and $C_2H_4$ sea–air fluxes represent the minimum degradation rate of these phosphonates, we further estimated the turnover time of phosphonates as 3.9 yr at Sta. 2 and 0.60–0.75 yr at Sta. 4 and 7.

### $CH_4$ and $C_2H_4$ production in seawater samples amended with phosphonates

The incubation experiments designed to test the capacity of surface microbial communities to metabolize phosphonates were conducted with seawater collected in the nutrient-rich shelf waters (Sta. 1), in waters immediately south of the Gulf Stream (Sta. 3), and in the oligotrophic Sargasso Sea (Sta. 4 and 5) (Fig. 5a–c). In all experiments, seawater was amended with inorganic N to alleviate N limitation. $CH_4$ and $C_2H_4$ were expected from the degradation of MPn and 2-HEP, respectively. The assays tested if the accumulation of $CH_4$ and $C_2H_4$ was significantly higher than in control samples amended only with inorganic N. Because the incubation time differed in some stations, the $CH_4$ and $C_2H_4$ concentrations were normalized by the length of the incubation period. The incubation conditions for each experiment are described in Table 3.

When seawater was supplemented with MPn and/or 2-HEP, inorganic N, and glucose, $CH_4$ and $C_2H_4$ production were significantly enhanced in all stations relative to controls ($p < 0.05$, one-tailed *t*-test; Fig. 5a). Assuming 100% conversion efficiency of MPn to $CH_4$ and 2-HEP to $C_2H_4$, 46–78% of MPn and 60–80% of 2-HEP were consumed. When seawater was amended with inorganic N and glucose, a significant production of $CH_4$ and $C_2H_4$ ($230 \pm 60$ pmol $L^{-1}$ $d^{-1}$ and $150 \pm 30$ pmol $L^{-1}$ $d^{-1}$, respectively; $p = 0.019$ and $p = 0.013$, one-tailed *t*-test) was detected only in Sta. 1 (Fig. 5b). When seawater was amended with MPn and/or 2-HEP and inorganic N (no glucose added), $CH_4$ and $C_2H_4$ production were significant only in Sta. 3, 4, and 5 ($p < 0.05$, one-tailed *t*-test) (Fig. 5c). When samples were supplied with equal concentrations of MPn and 2-HEP (Sta. 4 and 5), comparable amounts of $CH_4$ and $C_2H_4$ were produced (Fig. 5c).

**Table 3** Incubation conditions of surface seawater samples amended with MPn and/or 2-HEP.

| Station | Phosphonate | Depth (m) | Time (d) | Temp. (°C) |
|---|---|---|---|---|
| 1 | MPn | 10 | 4.0 | 13 |
| 3 | MPn | 10 | 7.8 | 18–24 |
| 4 | MPn | 16 | 6.5 | 22–23 |
| | 2-HEP | | | |
| 5 | MPn | 20 | 4.7 | 23–24 |
| | 2-HEP | | | |

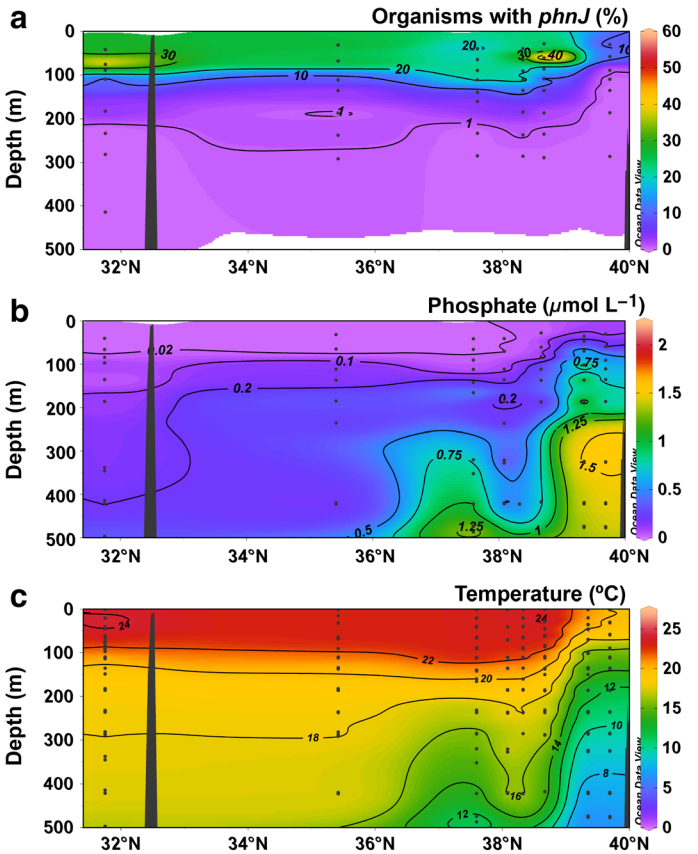


**Fig 6** Latitudinal and depth distribution of C-P lyase gene *phnJ* relative abundance, phosphate concentration, and temperature in the western North Atlantic Ocean during GEOTRACES Section GA03. (**a**) C-P lyase relative abundance is based on the analysis of metagenomes sampled during the GEOTRACES Section GA03 (Fig. 1) and is expressed as the percentage of organisms containing a copy of gene *phnJ*. (**b**) The corresponding section depicting phosphate concentrations ($\mu$mol $L^{-1}$). (**c**) The corresponding temperature section depicting colder water near the continental margin and warmer water in the Sargasso Sea. The gray symbols indicate the latitude and depth of discrete samples. For geographic reference, the bathymetry along the continental margin and Bermuda (latitude 32.3°N) is represented as gray shading.

### Bacterial degradation of HMWDOM phosphonates

The C-P lyase-containing bacterium *P. stutzeri* strain HI00D01 degraded similar amounts of MPn and 2-HEP of

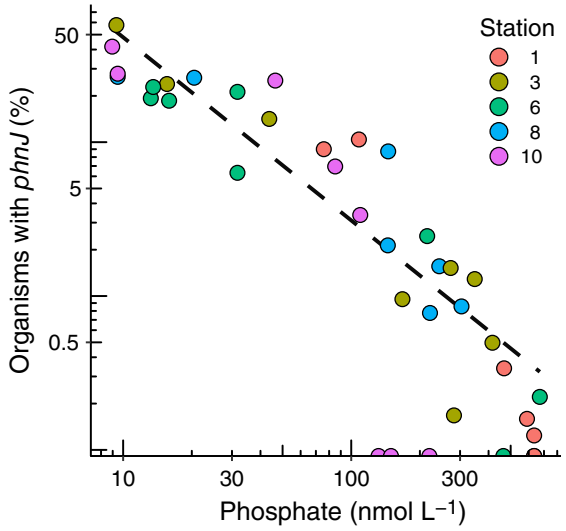


**Fig 7** Relationship between C-P lyase gene *phnJ* abundance and phosphate in the western North Atlantic Ocean. The abundance of the C-P lyase gene is expressed as the percentage of organisms possessing a copy of *phnJ* and was calculated for a subset of metagenomes of GEOTRACES Section GA03 (Fig. 1; Supporting Information Table S1). Data are color-coded by station. GA03 Sta. 4 was omitted from the analysis because high-sensitivity, low level phosphate measurements were not available. Phosphate concentration corresponding to the sampling depth of each metagenome was predicted by linear interpolation in each station profile because the latter did not always match exactly the depths at which seawater samples were collected for nutrient analysis. The dashed line depicts a linear regression model of *phnJ* abundance and Pi.

Sargasso Sea HMWDOM as shown by the production of $CH_4$ and $C_2H_4$ (Fig. 5d). The net concentrations of $CH_4$ and $C_2H_4$ produced were not significantly different ($p = 0.73$, *t*-test) and the mean ratio of $CH_4$ to $C_2H_4$ concentrations produced was 1.16.

### Abundance and distribution of C-P lyase

Our analysis of GEOTRACES metagenomes representative of the western North Atlantic Ocean in November 2011 revealed the prevalence of C-P lyase gene *phnJ* in the upper 100 m in the Sargasso Sea relative to deeper waters (Fig. 6). The percentage of organisms with C-P lyase gene *phnJ* ranged from 14% to 58% in the upper 100 m and declined to 0–10% in waters north of the Gulf Stream. The latitudinal gradient in *phnJ* relative abundance was similar to the distribution of $\Delta CH_4$ and $\Delta C_2H_4$ and opposite to the distribution of Pi and N + N concentrations observed in the AR16 cruise. The log-transformed *phnJ* relative abundance followed a significant inverse relationship with log-transformed Pi concentration ($r^2 = 0.85$, $F_{1,30} = 177.6$, $p << 0.01$) (Fig. 7). The log-transformed *phnJ* relative abundance was also significantly correlated with temperature ($r^2 = 0.81$, $F_{1,30} = 132.4$, $p << 0.01$) as expected from the distribution of Pi concentrations with respect to temperature (Supporting Information Fig. S1).

## Discussion

In this study, we tested the hypothesis that $CH_4$ and $C_2H_4$ supersaturation in the upper ocean is linked to the metabolism of phosphonates (MPn and 2-HEP, respectively) present in HMWDOM, a process regulated to a large extent by the concentration of Pi. The AR16 cruise took place in the spring and sampled waters with a gradient of Pi concentrations, from Pi-rich waters of the continental shelf and Gulf Stream, to the oligotrophic waters of the Sargasso Sea near Bermuda (Fig. 2). We identified several lines of evidence that indicate phos-phonate degradation is an important source of $CH_4$ and $C_2H_4$ in this ocean region. In the Pi-depleted Sargasso Sea surface waters, the concentrations of $CH_4$ and $C_2H_4$ in excess of solubility equilibrium were highly correlated and typically occurred at an approximate 1:1 ratio (Table 1 and Fig. 3), a value that approximates the 1:1 molar ratio of MPn to 2-HEP in Sargasso Sea HMWDOM. When natural bacterial communities were given a 1:1 mix of MPn and 2-HEP, $CH_4$ and $C_2H_4$ were produced in a 1:1 ratio indicating no selective degradation of either phosphonate (Fig. 5a–c). When HMWDOM was degraded by the C-P lyase-containing bacterium *P. stutzeri*, $CH_4$ and $C_2H_4$ were also produced in a 1:1 ratio indicating MPn and 2-HEP polysaccharides esters have similar bioavailabilities (Fig. 5d). Collectively, these observations point to a common production pathway of $CH_4$ and $C_2H_4$ in Sargasso Sea surface waters consistent with C-P lyase-mediated degradation of MPn and 2-HEP, the two most abundant phosphonate esters identified in HMWDOM (Repeta et al. 2016).

We also obtained evidence that Pi concentration plays an important role in the cycling of phosphonates. With the exception of $CH_4$ supersaturation in the shallow shelf waters, we observed an inverse relationship between Pi concentrations and $CH_4$ and $C_2H_4$ supersaturations along the cruise transect, suggesting that phosphonate degradation becomes more prominent as Pi availability decreases (Fig. 3). The high values of $CH_4$ supersaturation that we observed on the New England shelf may have originated from $CH_4$ seeps commonly found throughout the North Atlantic continental margin seafloor (Fig. 1; Skarke et al. 2014). In addition, MPn and 2-HEP were more readily degraded in Pi-depleted Sargasso Sea surface waters than in Pi-rich near-shore waters (Fig. 5c). Finally, in the Pi-depleted Sargasso Sea surface waters, the C-P lyase *phnJ* gene was present in a large proportion of the microbial community (Fig. 6) and its abundance followed an inverse relationship with Pi concentrations (Fig. 7). The depletion of Pi in Sargasso Sea surface waters thus leads to phosphonate degradation and contributes to the supersaturations of $CH_4$ and $C_2H_4$.

Phosphonate degradation captures the major trends of $CH_4$ and $C_2H_4$ saturation state in our study region and is most likely a major source of these gases. These results are consistent with the prominent role DOP plays in providing P to organisms, particularly in the Sargasso Sea (Lomas et al. 2010;

McLaughlin et al. 2013) and in other oligotrophic marine environments (Björkman and Karl 2003), and indicate that bacterial degradation of phosphonates is an important P acquisition pathway in this region. The prevalence of MPn and 2-HEP in HMWDOM (Repeta et al. 2016) and the enrichment of C-P lyase in marine bacterial communities inhabiting low Pi environments (Coleman and Chisholm 2010; Martinez et al. 2010; Sosa et al. 2019) lend further support to this hypothesis. But given that $CH_4$ and $C_2H_4$ supersaturations did not always follow a 1:1 ratio, additional sources of $CH_4$ cannot be ruled out.

### Phosphonate degradation potential of bacterial communities

The seawater incubation experiments performed during cruise AR16 also served to evaluate the phosphonate-degradation potential of native bacterial populations. Without exception, seawater amended with inorganic N, glucose, and phosphonates produced copious $CH_4$ and $C_2H_4$ from MPn and 2-HEP (Fig. 5a), confirming that bacteria possessing C-P lyase are ubiquitous in marine waters (Villarreal-Chiu et al. 2012; Sosa et al. 2019). Adding inorganic N and glucose, without the addition of phosphonates in the incubations, elicited gas production in shelf waters (Sta. 1), most likely from the degradation of phosphonates in native DOP, which was not the case in Sargasso Sea samples (Sta. 3 and 4; Fig. 5b). On the other hand, adding inorganic N and MPn (or 2-HEP) without glucose resulted in significantly higher gas production in the Sargasso Sea samples than in the shelf waters (Fig. 5c).

These regional patterns of $CH_4$ and $C_2H_4$ production may be explained by differences in the metabolic characteristics of the bacterial populations containing C-P lyase. For example, in Sargasso Sea surface waters, up to half of *Pelagibacter* clade organisms may encode C-P lyase (Coleman and Chisholm 2010; Carini et al. 2014; Sosa et al. 2019), but the vast majority lack the glycolysis pathway (Schwalbach et al. 2010). Therefore, in Sargasso Sea surface waters, it is possible that the addition of organic carbon compounds other than glucose would have promoted the growth of phosphonate-degrading bacteria in the incubations without added MPn and 2-HEP despite the apparent P limitation. The opposite is true for shelf water, where consumption of phosphonates in native DOP can be stimulated by the addition of an external carbon source such as glucose. Temperature differences between shelf waters and Sargasso Sea surface waters may also influence these observations but a temperature effect was not evident in experiments in which samples were amended with glucose, inorganic N, and phosphonates (Fig. 5a). Together this is interpreted to indicate that in shelf waters phosphonates may contribute to water column production of $CH_4$ and $C_2H_4$, albeit at slower rates than in the Pi-depleted Sargasso Sea surface waters, where bacteria more readily metabolize phosphonates.

### Alternate sources of $C_2H_4$

Until recently, the process underlying $C_2H_4$ supersaturation in the marine environment remained elusive. Ethylene derived from methionine metabolism serves an important role as a growth and development hormone in higher plants (Iqbal et al. 2017). Shaw (2001) investigated the production of non-$CH_4$ hydrocarbons in representative marine photosynthetic organisms including the cyanobacteria *Prochlorococcus* and *Synechococcus*, and the eukaryotic algae *Emiliania huxleyi*, *Micromonas pusilla*, and *Pelagomonas calceolate* but found no evidence of significant production of $C_2H_4$. In a study of dissolved hydrocarbons in the subtropical North Atlantic, Seifert et al. (1999) observed $C_2H_4$ maxima below the surface mixed layer, near the depth of the DCM, but did not identify a proportional relationship between the concentration of $C_2H_4$ and chlorophyll. In the region of the Sargasso Sea covered by our study, maximum concentrations of $C_2H_4$ often occurred below the surface mixed layer and coincided with the $CH_4$ maximum, well above the DCM (Fig. 4). Photo-degradation of DOM in seawater can also produce $C_2H_4$ (Ratte et al. 1993). In the case of light-dependent $C_2H_4$ production from DOM, higher concentrations of $C_2H_4$ would be expected near the surface and to scale proportionally with DOC concentrations. However, Seifert et al. (1999) found no correspondence between $C_2H_4$ and DOC or $C_2H_4$ and the time of day. The marked increase of $C_2H_4$ concentrations in Sargasso Sea surface waters relative to coastal waters, particularly where Pi concentrations were $< 50$ nmol $L^{-1}$, and its correspondence with $CH_4$ concentrations strongly suggest that $C_2H_4$ production is tightly linked to the degradation of phos-phonates in HMWDOM, specifically to the turnover of 2-HEP by C-P lyase as inferred by Repeta et al. (2016).

### Distribution of $CH_4$ and $C_2H_4$ supersaturation in the water column

In the Sargasso Sea sites, $\Delta CH_4$ and $\Delta C_2H_4$ often featured a concentration maximum in the interior of the euphotic zone, below the surface mixed layer (Fig. 4). Tilbrook and Karl (1995) suggested that in the open ocean the $CH_4$ subsurface maximum layer is the result of loss of $CH_4$ by gas exchange at the surface and limited diffusive flux of $CH_4$ below the surface mixed layer rather than of higher rates of in situ $CH_4$ production in that layer. Similarly, a mass balance of dissolved $CH_4$ in a mesotrophic lake concluded that the $CH_4$ maximum below the surface mixed layer is a result of wind-driven gas exchange at the surface, which promotes the outward flux of $CH_4$, and low turbulent mixing within the thermocline, which limits eddy vertical diffusivity and promotes local accumulation of $CH_4$ (Donis et al. 2017). In the region below the surface mixed layer in the open ocean and lakes, the vertical eddy diffusivity approximates an inverse relationship with water column stratification expressed as buoyancy frequency, $N$ (Quay et al. 1980; Law et al. 2001). At our Sargasso Sea study sites, the presence of a peak of excess $CH_4$ and $C_2H_4$

concentration in the layer of highest $N$ at the base of the surface mixed layer is consistent with this physical model and suggests that the concentrations of $CH_4$ and $C_2H_4$ are sensitive to the vertical density structure of the water column (Fig. 4). At one of our sampling sites (Sta. 6), for example, a DCM was clearly present at 125 m but both $CH_4$ and $C_2H_4$ concentrations were uniformly distributed in the upper 100 m due to a weakened thermocline (Fig. 4). Assuming that phosphonate degradation rates remain constant from the surface to a depth of 100–200 m in the Sargasso Sea where Pi is depleted, the loss of $CH_4$ and $C_2H_4$ to the atmosphere at the surface and the increased stratification below the surface mixed layer may give rise to the maximum in $CH_4$ and $C_2H_4$.

### Mass balance of $CH_4$ and $C_2H_4$ sea-air flux and phosphonate turnover

The comparable $CH_4$ and $C_2H_4$ sea–air flux estimates at several sites sampled in the Sargasso Sea suggests that MPn and 2-HEP have similar bioavailabilities and turnover rates. This result was consistent with the bioavailability of MPn and 2-HEP in HMWDOM inferred from the equal release of $CH_4$ and $C_2H_4$ by *P. stutzeri* cultures (Fig. 5d) and by the production of $CH_4$ and $C_2H_4$ from the degradation of HMWDOM by microbial communities at Sta. ALOHA (Repeta et al. 2016). Assuming the main sink of $CH_4$ and $C_2H_4$ in Sargasso Sea surface waters is loss to the atmosphere, the sea–air flux estimates for these trace gases may approximate the steady-state turnover rates of MPn and 2-HEP in the surface mixed layer.

At Sta. ALOHA (22°45′N, 158°W) in the North Pacific Subtropical Gyre, Repeta et al. (2016) estimated that a daily turnover of as little as 0.25% of the MPn inventory, equivalent to a MPn residence time of 1–2 yr, was sufficient to balance the measured $CH_4$ sea–air flux (1.6–2.5 $\mu$mol $m^{-2}$ $d^{-1}$) and to sustain $CH_4$ supersaturation in the euphotic zone. Using this approach, we estimated a residence time of HMWDOM phosphonates of 0.60–0.75 yr in Sargasso Sea surface waters. This relatively long residence time is comparable to the estimated MPn residence time at Sta. ALOHA even though less than 1% of organisms possess C-P lyase at Sta. ALOHA (Sosa et al. 2017) compared to $\sim$ 50% of organisms in the Sargasso Sea. However, at Sta. ALOHA surface waters (0–100 m), the average DOP concentrations are 268 nmol $L^{-1}$ (Björkman and Karl 2003) while at the Bermuda Atlantic Time-series (BATS) station in the Sargasso Sea, surface waters (0–100 m) average DOP concentrations of only 61 nmol $L^{-1}$ (Lomas et al. 2010), approximately fourfold lower than at Sta. ALOHA. Thus, it is possible that differences in the phosphonate inventory and the phosphonate supply/production rates between these ecosystems result in similar phosphonate turnover times. Because HMWDOM phosphonates occur as polysaccharide esters, their turnover rate is also tied to the cycling of HMWDOM (Repeta et al. 2016), in addition to the availability of Pi. These results suggest that HMWDOM phosphonates fit the role of semi-labile pools of DOP that support export production in the North Atlantic Subtropical Gyre (Torres-Valdés et al. 2009; Lomas et al. 2010).

## Conclusion

Collectively, our results indicate that HMWDOM phosphonates are an important source of $CH_4$ and $C_2H_4$ in the Sargasso Sea. These results also indicate that Pi concentration can be an important control on the saturation state of $CH_4$ and $C_2H_4$ in marine surface waters. Thus, phosphonates represent a bioavailable source of P in Pi-depleted environments like the Sargasso Sea as has been inferred by the prevalence of phos-phonate transport and degradation pathways in microbial communities in low Pi ocean regions. While Pi depletion promotes phosphonate degradation and contributes to $CH_4$ and $C_2H_4$ supersaturation, the instantaneous flux of these trace gases to the atmosphere is also controlled to a great extent by the regional wind regime, water column mixing, and possibly by the phosphonate inventory in surface waters. In ocean ecosystems with different trophic regimes, other sources of $CH_4$ and $C_2H_4$ may be equally or more important than phos-phonate degradation. In the shallow, Pi-rich New England shelf waters, the discrepancy between $CH_4$ and $C_2H_4$ concentrations and sea–air fluxes points to additional $CH_4$ sources or pathways that are independent of phosphonates and C-P lyase. Geological $CH_4$ is likely an important source due to the presence of gas seeps along the continental margin. Direct measurements of C-P lyase activity and detailed investigations of additional sources and sinks of phosphonates, $CH_4$, and $C_2H_4$ will help provide a more thorough understanding of the cycling of phosphonates and of these trace hydrocarbon gases in the upper ocean.

## Data Availability Statement

Nutrient and gas concentration data from this study are publicly available through NSF's Biological and Chemical Oceanography Data Management Office (BCO-DMO) under project 765014.

## References

Bentamy, A., and D. Croize Fillon. 2012. Gridded surface wind fields from Metop/ASCAT measurements. Int. J. Remote Sens. **33**: 1729–1754. doi:10.1080/01431161.2011.600348

Bernal, E. 2014. Limit of detection and limit of quantification determination in gas chromatography, p. 57–81. *In* X. Guo [ed.], Advances in gas chromatography. IntechOpen. doi: 10.5772/57341

Biller, S. J., and others. 2018. Marine microbial metagenomes sampled across space and time. Sci. Data **5**: 180176. doi:10.1038/sdata.2018.176

Björkman, K., and D. M. Karl. 2003. Bioavailability of dissolved organic phosphorus in the euphotic zone at Station

ALOHA, North Pacific Subtropical Gyre. Limnol. Oceanogr. **48**: 1049–1057. doi:10.4319/lo.2003.48.3.1049

Bolger, A. M., M. Lohse, and B. Usadel. 2014. Trimmomatic: A flexible trimmer for Illumina sequence data. Bioinformatics **30**: 2114–2120. doi:10.1093/bioinformatics/btu170

Born, D. A., E. C. Ulrich, K. S. Ju, S. C. Peck, W. A. van der Donk, and C. L. Drennan. 2017. Structural basis for methylphosphonate biosynthesis. Science **358**: 1336–1339. doi:10.1126/science.aao3435

Breitbarth, E., M. M. Mills, G. Friedrichs, and J. LaRoche. 2004. The Bunsen gas solubility coefficient of ethylene as a function of temperature and salinity and its importance for nitrogen fixation assays. Limnol. Oceanogr.: Methods **2**: 282–288. doi:10.4319/lom.2004.2.282

Carini, P., A. E. White, E. O. Campbell, and S. J. Giovannoni. 2014. Methane production by phosphate-starved SAR11 chemoheterotrophic marine bacteria. Nat. Commun. **5**: 1–8. doi:10.1038/ncomms5346

Cavendar-Bares, K. K., D. M. Karl, and S. W. Chisholm. 2001. Nutrient gradients in the western North Atlantic Ocean: Relationship to microbial community structure and comparison to patterns in the Pacific Ocean. Deep-Sea Res. I **48**: 2373–2395. doi:10.1016/S0967-0637(01)00027-9

Clark, L. L., and E. D. Ingall. 1998. Marine phosphorus is selectively remineralized. Nature **393**: 426. doi:10.1038/30881

Coleman, M. L., and S. W. Chisholm. 2010. Ecosystem-specific selection pressures revealed through comparative population genomics. Proc. Natl. Acad. Sci. USA **107**: 18634–18639. doi:10.1073/pnas.1009480107

Cotner, J. B., J. W. Ammerman, E. R. Peele, and E. Bentzen. 1997. Phosphorus-limited bacterioplankton growth in the Sargasso Sea. Aquat. Microb. Ecol. **13**: 141–149. doi:10.3354/ame013141

Damm, E., E. Helmke, S. Thoms, U. Schauer, E. Othig, K. Bakker, and R. P. Kiene. 2009. Methane production in aerobic oligotrophic surface water in the central Arctic Ocean. Biogeosciences **6**: 10355–10379. doi:10.5194/bgd-6-10355-2009

de Angelis, M. A., and C. Lee. 1994. Methane production during zooplankton grazing on marine phytoplankton. Limnol. Oceanogr. **39**: 1298–1308. doi:10.4319/lo.1994.39.6.1298

Donis, D., S. Flury, A. Stöckli, J. E. Spangenberg, D. Vachon, and D. F. McGinnis. 2017. Full-scale evaluation of methane production under oxic conditions in a mesotrophic lake. Nat. Commun. **8**: 1–11. doi:10.1038/s41467-017-01648-4

Dyhrman, S., J. Ammerman, and B. van Mooy. 2007. Microbes and the marine phosphorus cycle. Oceanography **20**: 110–116. doi:10.5670/oceanog.2007.54

Eddy, S. R. 2009. A new generation of homology search tools based on probabilistic inference. Genome Inform. **23**: 205–211. doi:10.1142/9781848165632_0019

Florez-Leiva, L., E. Damm, and L. Farías. 2013. Methane production induced by dimethylsulfide in surface water of an upwelling ecosystem. Prog. Oceanogr. **112–113**: 38–48. doi:10.1016/j.pocean.2013.03.005

Foreman, R. K., M. Segura-Noguera, and D. M. Karl. 2016. Validation of Ti(III) as a reducing agent in the chemiluminescent determination of nitrate and nitrite in seawater. Mar. Chem. **186**: 83–89. doi:10.1016/j.marchem.2016.08.003

Foreman, R. K., K. M. Björkman, C. A. Carlson, K. Opalk, and D. M. Karl. 2019. Improved ultraviolet photo-oxidation system yields estimates for deep-sea dissolved organic nitrogen and phosphorus. Limnol. Oceanogr.: Methods **17**: 277–291. doi:10.1002/lom3.10312

Goldman, J. C., D. A. Caron, and M. R. Dennett. 1987. Regulation of gross growth efficiency and ammonium regeneration in bacteria by substrate C:N ratio. Limnol. Oceanogr. **32**: 1239–1252. doi:10.4319/lo.1987.32.6.1239

Gundersen, K., M. Heldal, S. Norland, D. A. Purdie, and A. H. Knap. 2002. Elemental C, N, and P cell content of individual bacteria collected at the Bermuda Atlantic Time-series Study (BATS) site. Limnol. Oceanogr. **47**: 1525–1530. doi:10.4319/lo.2002.47.5.1525

Hovland, M., A. G. Judd, and R. A. J. Burke. 1993. The global flux of methane from shallow submarine sediments. Chemosphere **26**: 559–578. doi:10.1016/0045-6535(93)90442-8

Hyatt, D., G.-L. Chen, P. F. Locascio, M. L. Land, F. W. Larimer, and L. J. Hauser. 2010. Prodigal: Prokaryotic gene recognition and translation initiation site identification. BMC Bioinformatics **11**: 119. doi:10.1186/1471-2105-11-119

Iqbal, N., N. A. Khan, A. Ferrante, A. Trivellini, A. Francini, and M. I. R. Khan. 2017. Ethylene role in plant growth, development and senescence: Interaction with other phytohormones. Front. Plant Sci. **8**: 475. doi:10.3389/fpls.2017.00475

Johnson, M. T. 2010. A numerical scheme to calculate temperature and salinity dependent air-water transfer velocities for any gas. Ocean Sci. **6**: 913–932. doi:10.5194/os-6-913-2010

Kara, A. B., P. A. Rochford, and H. E. Hurlburt. 2000. An optimal definition for ocean mixed layer depth. J. Geophys. Res. Oceans **105**: 16803–16821. doi:10.1029/2000JC900072

Karl, D. M. 2014. Microbially mediated transformations of phosphorus in the sea: New views of an old cycle. Ann. Rev. Mar. Sci. **6**: 279–337. doi:10.1146/annurev-marine-010213-135046

Karl, D. M., and G. Tien. 1992. MAGIC: A sensitive and precise method for measuring dissolved phosphorus in aquatic environments. Limnol. Oceanogr. **37**: 105–116. doi:10.4319/lo.1992.37.1.0105

Karl, D. M., and B. D. Tilbrook. 1994. Production and transport of methane in oceanic particulate organic matter. Nature **368**: 732–734. doi:10.1038/368732a0

Karl, D. M., L. Beversdorf, K. M. Björkman, M. J. Church, A. Martinez, and E. F. DeLong. 2008. Aerobic production of

methane in the sea. Nat. Geosci. **1**: 473–478. doi:10.1038/ngeo234

Kiene, R. P. 1991. Production and consumption of methane in aquatic systems, p. 111–146. *In* W. B. Rogers and J. E. Whitman [eds.], Microbial production and consumption of greenhouse gases: Methane, nitrogen oxides and halomethanes. American Society for Microbiology.

Kolowith, L. C., E. D. Ingall, and R. Benner. 2001. Composition and cycling of marine organic phosphorus. Limnol. Oceanogr. **46**: 309–320. doi:10.4319/lo.2001.46.2.0309

Krom, M. D., K. C. Emeis, and P. Van Cappellen. 2010. Why is the Eastern Mediterranean phosphorus limited? Prog. Oceanogr. **85**: 236–244. doi:10.1016/j.pocean.2010.03.003

Lamontagne, R. A., J. W. Swinnerton, V. J. Linnenbom, and W. D. Smith. 1973. Methane concentrations in various marine environments. J. Geophys. Res. **78**: 5317–5324. doi:10.1029/JC078i024p05317

Langmead, B., and S. L. Salzberg. 2012. Fast gapped-read alignment with Bowtie 2. Nat. Methods **9**: 357–359. doi:10.1038/nmeth.1923

Law, C. S., A. P. Martin, M. I. Liddicoat, A. J. Watson, K. J. Richards, and E. M. S. Woodward. 2001. A Lagrangian SF6 tracer study of an anticyclonic eddy in the North Atlantic: Patch evolution, vertical mixing and nutrient supply to the mixed layer. Deep-Sea Res. Part II Top. Stud. Oceanogr. **48**: 705–724. doi:10.1016/S0967-0645(00)00112-0

Lenhart, K., T. Klintzsch, G. Langer, G. Nehrke, M. Bunge, S. Schnell, and F. Keppler. 2015. Evidence for methane production by marine algae *Emiliania huxleyi* and its implication for the methane paradox in oxic waters. Biogeosci. Discuss. **12**: 20323–20360. doi:10.5194/bgd-12-20323-2015

Lomas, M. W., A. L. Burke, D. A. Lomas, D. W. Bell, C. Shen, S. T. Dyhrman, and J. W. Ammerman. 2010. Sargasso Sea phosphorus biogeochemistry: An important role for dissolved organic phosphorus (DOP). Biogeosciences **7**: 695–710. doi:10.5194/bg-7-695-2010

Martinez, A., G. W. Tyson, and E. F. DeLong. 2010. Widespread known and novel phosphonate utilization pathways in marine bacteria revealed by functional screening and metagenomic analyses. Environ. Microbiol. **12**: 222–238. doi:10.1111/j.1462-2920.2009.02062.x

Marty, D. 1993. Methanogenic bacteria in seawater. Limnol. Oceanogr. **38**: 452–456. doi:10.4319/lo.1993.38.2.0452

McLaughlin, K., J. A. Sohm, G. A. Cutter, M. W. Lomas, and A. Paytan. 2013. Phosphorus cycling in the Sargasso Sea: Investigation using the oxygen isotopic composition of phosphate, enzyme-labeled fluorescence, and turnover times. Global Biogeochem. Cycles **27**: 375–387. doi:10.1002/gbc.20037

Metcalf, W. W., and others. 2012. Synthesis of methylphosphonic acid by marine microbes: A source for methane in the aerobic ocean. Science **337**: 1104–1107. doi:10.1126/science.1219875

Moore, C. M., and others. 2013. Processes and patterns of oceanic nutrient limitation. Nat. Geosci. **6**: 701–710. doi:10.1038/ngeo1765

Obernosterer, I., N. Kawasaki, and R. Benner. 2003. P-limitation of respiration in the Sargasso Sea and uncoupling of bacteria from P-regeneration in size-fractionation experiments. Aquat. Microb. Ecol. **32**: 229–237. doi:10.3354/ame032229

Pante, E., and B. Simon-Bouhet. 2013. marmap: A package for importing, plotting and analyzing bathymetric and topographic data in R. PLoS One **8**: e73051. doi:10.1371/journal.pone.0073051

Quay, P. D., W. S. Broecker, and R. H. Hesslein. 1980. Vertical diffusion rates determined by tritium tracer experiments in the thermocline and hypolimnion of two lakes. Limnol. Oceanogr. **25**: 201–218. doi:10.4319/lo.1980.25.2.0201

Quinlan, A. R., and I. M. Hall. 2010. BEDTools: A flexible suite of utilities for comparing genomic features. Bioinformatics **26**: 841–842. doi:10.1093/bioinformatics/btq033

Ratte, M., C. Plass-Dülmer, R. Koppman, J. Rudolph, and J. Denga. 1993. Production mechanisms of C2-C4 hydrocarbons in seawater: Field measurements and experiments. Global Biogeochem. Cycles **7**: 369–378. doi:10.1029/93GB00054

Reeburgh, W. 2007. Oceanic methane biogeochemistry. Chem. Rev. **107**: 486–513. doi:10.1021/cr050362v

Repeta, D. J., S. Ferrón, O. A. Sosa, C. G. Johnson, L. D. Repeta, M. Acker, E. F. DeLong, and D. M. Karl. 2016. Marine methane paradox explained by bacterial degradation of dissolved organic matter. Nat. Geosci. **9**: 884–887. doi:10.1038/ngeo2837

Rudolph, J., and D. H. Ehhalt. 1981. Measurements of $C_2$-$C_5$ hydrocarbons over the North Atlantic. J. Geophys. Res. **86**: 959–964. doi:10.1029/JC086iC12p11959

Schlitzer, R. 2018. Ocean Data View. Available from odv.awi.de [accessed 2019 October 28].

Schlitzer, R., and others. 2018. The GEOTRACES intermediate data product 2017. Chem. Geol. **493**: 210–223. doi:10.1016/j.chemgeo.2018.05.040

Schwalbach, M. S., H. J. Tripp, L. Steindler, D. P. Smith, and S. J. Giovannoni. 2010. The presence of the glycolysis operon in SAR11 genomes is positively correlated with ocean productivity. Environ. Microbiol. **12**: 490–500. doi:10.1111/j.1462-2920.2009.02092.x

Scranton, M. I., and P. G. Brewer. 1977. Occurrence of methane in the near-surface waters of the western subtropical North-Atlantic. Deep-Sea Res. **24**: 127–138. doi:10.1016/0146-6291(77)90548-3

Scranton, M. I., and J. W. Farrington. 1977. Methane production in the waters off Walvis Bay. J. Geophys. Res. **82**: 4947–4953. doi:10.1029/JC082i031p04947

Seifert, R., N. Delling, H. H. Richnow, S. Kempe, J. Hefter, and W. Michaelis. 1999. Ethylene and methane in the upper

water column of the subtropical Atlantic. Biogeochemistry **44**: 73–91. doi:10.1023/A:1006090917059

Shao, Z., and others. 2008. Biosynthesis of 2-hydroxyethylphosphonate, an unexpected intermediate common to multiple phosphonate biosynthetic pathways. J. Biol. Chem. **283**: 23161–23168. doi:10.1074/jbc.M801788200

Shaw, S. L. 2001. The production of non-methane hydrocarbons by marine plankton. Ph.D. thesis. Massachusetts Institute of Technology.

Skarke, A., C. Ruppel, M. Kodis, D. Brothers, and E. Lobecker. 2014. Widespread methane leakage from the sea floor on the northern US Atlantic margin. Nat. Geosci. **7**: 657–661. doi:10.1038/ngeo2232

Sosa, O. A., D. J. Repeta, S. Ferrón, J. A. Bryant, D. R. Mende, D. M. Karl, and E. F. DeLong. 2017. Isolation and characterization of bacteria that degrade phosphonates in marine dissolved organic matter. Front. Microbiol. **8**: 1–16. doi:10.3389/fmicb.2017.01786

Sosa, O. A., D. J. Repeta, E. F. DeLong, M. D. Ashkezari, and D. M. Karl. 2019. Phosphate-limited ocean regions select for bacterial populations enriched in the carbon-phosphorus lyase pathway for phosphonate degradation. Environ. Microbiol. **21**: 2402–2414. doi:10.1111/1462-2920.14628

Sunagawa, S., and others. 2013. Metagenomic species profiling using universal phylogenetic marker genes. Nat. Methods **10**: 1196–1199. doi:10.1038/nmeth.2693

Thingstad, T. F., and others. 2005. Nature of phosphorus limitation in the ultraoligotrophic eastern Mediterranean. Science **309**: 1068–1071. doi:10.1126/science.1112632

Thomson-Bulldis, A., and D. M. Karl. 1998. Application of a novel method for phosphorus determinations in the oligotrophic North Pacific Ocean. Limnol. Oceanogr. **43**: 1565–1577.

Tilbrook, B. D., and D. M. Karl. 1995. Methane sources, distributions and sinks from California coastal waters to the oligotrophic North Pacific gyre. Mar. Chem. **49**: 51–64. doi:10.1016/0304-4203(94)00058-L

Torres-Valdés, S., and others. 2009. Distribution of dissolved organic nutrients and their effect on export production over the Atlantic Ocean. Global Biogeochem. Cycles **23**: 1–16. doi:10.1029/2008GB003389

Van Wambeke, F., U. Christaki, A. Giannakourou, T. Moutin, and K. Souvemerzoglou. 2002. Longitudinal and vertical trends of bacterial limitation by phosphorus and carbon in the Mediterranean Sea. Microb. Ecol. **43**: 119–133. doi:10.1007/s00248-001-0038-4

Villarreal-Chiu, J. F., J. P. Quinn, and J. W. McGrath. 2012. The genes and enzymes of phosphonate metabolism by bacteria, and their distribution in the marine environment. Front. Microbiol. **3**: 1–13. doi:10.3389/fmicb.2012.00019

Wanninkhof, R. 2014. Relationship between wind speed and gas exchange over the ocean revisited. Limnol. Oceanogr.: Methods **12**: 351–362. doi:10.4319/lom.2014.12.351

Weber, T., N. A. Wiseman, and A. Kock. 2019. Global ocean methane emissions dominated by shallow coastal waters. Nat. Commun. **10**: 4584. doi:10.1038/s41467-019-12541-7

White, A. K., and W. W. Metcalf. 2007. Microbial metabolism of reduced phosphorus compounds. Annu. Rev. Microbiol. **61**: 379–400. doi:10.1146/annurev.micro.61.080706.093357

Wiesenburg, D. A., and N. L. Guinasso. 1979. Equilibrium solubilities of methane, carbon monoxide, and hydrogen in water and sea water. J. Chem. Eng. Data **24**: 356–360. doi:10.1021/je60083a006

Wilson, S. T., S. Ferrón, and D. M. Karl. 2017. Interannual variability of methane and nitrous oxide in the North Pacific Subtropical Gyre. Geophys. Res. Lett. **44**: 9885–9892. doi:10.1002/2017GL074458

Wu, J., W. G. Sunda, E. A. Boyle, and D. M. Karl. 2000. Phosphate depletion in the western North Atlantic Ocean. Science **289**: 759–762. doi:10.1126/science.289.5480.759

Young, C. L., and E. D. Ingall. 2010. Marine dissolved organic phosphorus composition: Insights from samples recovered using combined electrodialysis/reverse osmosis. Aquat. Geochem. **16**: 563–574. doi:10.1007/s10498-009-9087-y

## Acknowledgments

We thank the captain and crew of the R/V *Neil Armstrong* and chief scientist Benjamin Van Mooy for supporting and leading research at sea. Chiara Santinelli and Eric Grabowski provided analyses of dissolved organic carbon. This research was funded by NSF Chemical Oceanography award OCE-1634080 to D.J.R. Additional support was provided by the Gordon and Betty Moore Foundation grant 3794 to D.M.K. and grant 6000 to D.J.R., and the Simons Collaboration on Ocean Processes and Ecology (SCOPE) program grant 329108 to D.M.K., E.F.D., and D.J.R.

## Conflict of Interest

None declared.

*Submitted 27 June 2019*
*Revised 31 January 2020*
*Accepted 26 April 2020*

*Associate editor: Bo Thamdrup*